Atmos. Chem. Phys. Discuss., https://doi.org/10.5194/acp-2018-1229
Manuscript under review for journal Atmos. Chem. Phys.
Discussion started: 21 January 2019

Atmospheric Chemistry and Physics
Open Access
Discussions

Source apportionment of highly time resolved trace elements during a firework episode from a rural freeway site in Switzerland

Pragati Rai[1], Markus Furger[1], Jay Slowik[1], Francesco Canonaco[1], Roman Fröhlich[1], Christoph Hüglin[2], María Cruz Minguillón[3], Krag Petterson[4], Urs Baltensperger[1] and André S.H. Prévôt[1]

[1] Laboratory of Atmospheric Chemistry, Paul Scherrer Institute, Villigen PSI, 5232, Switzerland
[2]Laboratory for Air Pollution / Environmental Technology, Empa, 8600 Dübendorf, Switzerland
[3]Institute of Environmental Assessment and Water Research (IDAEA), CSIC, 08034 Barcelona, Spain
[4]Cooper Environmental Services (CES), 9403 SW Nimbus Avenue, Beaverton, OR 97008, USA

Correspondence to: André S. H. Prévôt (andre.prevot@psi.ch) and Markus Furger (markus.furger@psi.ch)

Abstract. Trace element measurements in PM_{10} were performed with 1 h time resolution at a rural freeway site during summer 2015 in Switzerland using the Xact multi-metals monitor. On average the Xact 625 elements (without accounting for oxygen and other associated elements) make up about 20 % of the total PM_{10} mass (14.6 µg m^{-3}). Subsequently, a source apportionment by positive matrix factorization (PMF) implemented via the Source Finder software (SoFi Pro) was applied. Eight different sources were identified (notable elements in brackets) for PM_{10}: fireworks-I (K, S, Ba, Cl), fireworks-II (K), sea salt (Cl), secondary sulfate (S), background dust (Si, Ti), road dust (Ca), traffic-related (Fe) and industrial (Zn, Pb). The major components were secondary sulfate and traffic-related followed by background dust and road dust factors, explaining 21 %, 20 %, 18 % and 16 % of the analysed PM_{10} elemental mass, respectively, with the factor mass not corrected for oxygen content. Further, there are minor contributions (on the order of a few percent) of sea salt and industrial sources. The regionally influenced secondary sulfate factor experiences negligible resuspension, and concentrations are similar throughout the day. The significant loads of the traffic-related and road dust factors with strong diurnal variations highlight the continuing importance of vehicle-related air pollutants at this site. Enhanced control of PMF using SoFi Pro allowed for a successful apportionment of transient sources such as the two firework factors and sea salt, which remained mixed when analysed by unconstrained PMF.

1 Introduction

Ambient particulate matter (PM) plays a major role in affecting human health and air quality. Trace elements represent a minor fraction of the atmospheric aerosol on a mass basis, but they can act as specific markers for several emission sources. The short- or long-term exposure of ambient particulate matter (PM) has significant negative effects on human health (Dao et al., 2012; Ancelet et al., 2012; Zhao and Hopke, 2004; Pope and Dockery, 2006; Dockery et al., 1993; Zhou et al., 2018). Cakmak et al. (2014) found significant association of acute changes in cardiovascular and respiratory physiology with $PM_{2.5}$ metals in Ontario, Canada. Metallic components of PM, especially the fine fraction of trace elements such as Fe, Ni, Cu, V, Pb and Zn appear to be a significant cause of both pulmonary and cardiovascular diseases (Kelly and Fussell, 2012). Airborne particles and associated trace elements originate from various emission sources, such as motor vehicles, power plants, construction activities, in a broad size range. Among them, traffic-related emissions are of particular interest (Brauer et al., 2002). Traffic-derived PM has high risk of respiratory illness, asthma and cardiovascular diseases, resulting in increased rate in mortality (Kelly and Fussell, 2011). Traffic-related PM is emitted mainly as exhaust emissions (tailpipe exhaust from gasoline and diesel engines) and non-exhaust emissions (resuspension of road dust and brake and tire wear emissions) (Lawrence et al., 2013; Lin et al., 2015; Thorpe and Harrison, 2008; Zhou et al., 2018; Grigoratos and Martini, 2015; Amato et al., 2014b; Bukowiecki et al., 2010). Exhaust emissions are predominantly in the fine fraction of PM whereas non-exhaust emissions contribute mostly to the coarse fraction (Amato et al., 2011; Thorpe and Harrison, 2008). Exhaust emission-related elements are comprised of Pb, Zn, Ni and V (Lin et al., 2015; Minguillon et al., 2012), while the non-exhaust emissions are dominated by Fe, Cu, Ba, Ca, Sb, Sn, Cr and Zn from brake lining and tire wear. The presence of Fe in brake lining can reach up to 60 % by weight. Brake pads are usually filled with $BaSO_4$ while Sb, Sn and Mo sulfides are often added as lubricants and Cu, Cr and Zn are major additives to lubricating oils and normally used to improve friction (Thorpe and Harrison, 2008; Amato et al., 2014a). Sb has been identified as a major tracer of brake wear, due to significant (1–5 %) percentage of Sb in brake linings in the form of stibnite (Sb_2S_3) (Grigoratos and Martini, 2015; Bukowiecki et al., 2009). It has been reported that asphalt pavement-induced particles were characterized mainly by high concentrations of Cu, Cr, Ni, As and Pb (Yu, 2013) as well as Ca, Si, Mg, Al, Fe, P, S, Cl, K, V, Mn, Na (Fullova et al., 2017). Therefore, it is important to monitor traffic emissions for health risk assessment, the study of which relies heavily on the source apportionment (SA) of PM using chemically speciated data (Zhou et al., 2018).

Source quantification and characterization is an important step in understanding the relationship between source emissions, ambient concentrations, and health and environmental effects. SA by receptor models has been widely used in recent years to identify and apportion the contributions of various sources to the airborne PM concentrations. Positive Matrix Factorization (PMF) is one of the most widely used receptor models for SA of trace elements (Rahman et al., 2011; Ancelet et al., 2012; Cesari et al., 2014; Ducret-Stich et al., 2013; Kim et al., 2003; Rai et al., 2016; Zhang et al., 2013; Harrison et al., 2011; Hedberg et al., 2005). However, a very limited number of studies are available for trace elements emission sources with high time resolution (hourly or sub-hourly) (Visser et al., 2015; Crilley et al., 2016; Bukowiecki et al., 2010; Richard et al., 2011; Dall'Osto et al., 2013; Manousakas et al., 2015; Jeong et al., 2019; Wang et al., 2018). Hourly trace elements data can be used to explore the diurnal patterns of emissions from traffic, biomass burning and industrial sources, and thereby yielding more accurate and exposure-relevant SA results. Currently, there are very few instruments available for the field sampling of trace elements with high time resolution such as the rotating drum impactor (RDI) (Bukowiecki et al., 2008), the streaker sampler (PIXE International Corporation) (Lucarelli et al., 2011) and the semi-continuous elements in aerosol sampler (SEAS) (Kidwell and Ondov, 2001). The large quantity of samples generated by these samplers requires a labour intensive and time consuming offline analysis. These offline analysis needs synchrotron radiation X-ray fluorescence spectrometry (SR-XRF) of aerosol samples collected with a RDI, Particle induced X-ray emission (PIXE) with the streaker sampler and graphite furnace atomic absorption spectrometry (GFAAS) with the SEAS. A recently introduced online high time resolution instrument can collect samples and perform analysis for metals simultaneously in a near real time scenario without waiting for laboratory analysis. The Xact 625 and the newer 625i ambient metals monitors (Cooper Environmental Services, Beaverton, Oregon, USA) based on XRF have been developed in recent years and have been used in several field studies (Furger et al., 2017; Park et al., 2014; Tremper et al., 2018; Chang et al., 2018). However, only two studies included SA on Xact data (Park et al., 2014; Chang et al., 2018).

In the present study, we conducted SA using PMF to characterize the source emissions of highly time-resolved metals during a three-week campaign at a traffic-influenced site in Härkingen, Switzerland. PMF was implemented through the multilinear engine-2 (ME-2) solver and controlled via SoFi which allows for a comprehensive and systematic exploration of the solution space (Bozzetti et al., 2016; Canonaco et al., 2013). The later, being essential in particular when separating extreme events such as fireworks which are most often excluded from the PMF input matrix (Ducret-Stich et al., 2013; Norris et al., 2014) to avoid distortion in the PMF solution due to unusually high emissions. Although a few studies have already been carried out in the past at this location (Lanz et al., 2010; Hueglin et al., 2006; Furger et al., 2017), none of these studies have reported SA on trace elements.

2 Experimental setup and data analysis

2.1 Sampling location

PM_{10} sampling was performed from 23 July until 13 August 2015 in Härkingen, Switzerland, a permanent station of the Swiss Air Pollution Monitoring Network (NABEL). Extreme firework episodes were captured during the Swiss National Day Celebration (1 August). The site is situated next to the A1 freeway which is the main traffic route between eastern (Zurich) and western (Bern) Switzerland. The measurement site is bordered by agricultural areas to the west and north while there are villages in the south and east direction. There is a metal processing company to the south-east across the freeway which manufactures wheels for passenger cars and commercial vehicles, and some small scale industrial buildings to the north-west. The emissions reaching the measurement site depend on wind direction. The site is strongly influenced by local road traffic emissions when winds come from the southern sector, while the northern wind sector represents the air constituents from a rural area. A detailed description of the sampling site can be found in previous studies (Furger et al., 2017; Hueglin et al., 2006)

2.2 Sampling and analysis

Sampling and analysis was conducted with an Xact 625 ambient metals monitor (Cooper Environmental Services, Beaverton, Oregon, USA) equipped with a PM_{10} inlet. The instrument was set up to quantify 24 elements (Si, S, Cl, K, Ca, Ti, V, Cr, Mn, Fe, Co, Ni, Cu, Zn, As, Se, Cd, Sn, Sb, Ba, Pt, Hg, Pb and Bi) with 1 h time resolution. In addition, 24-h PM_{10} samples were collected by a Digital DA-80H HiVol sampler with quartz fiber filters. Ten of these 24-h PM_{10} samples were analysed by inductively coupled plasma optical emission spectrometry (ICP-OES) for the concentrations of Na, Mg, Al, P, S, K, Ca, Ti and Fe. Moreover, the station was equipped with other instruments such as a TEOM FDMS 8500 (tapered element oscillating microbalance), a multi angle absorption photometer (MAAP, Thermo 5012) and standard meteorological sensors (temperature, wind speed and direction, precipitation). Specifically for the campaign, a Q-ACSM (quadrupole aerosol chemical speciation monitor, Aerodyne Inc.) was deployed (Ng et al., 2011; Crenn et al., 2015) and the data were used for comparison of the factors during the SA analysis.

2.3 PMF using ME-2

Positive matrix factorization is one of the most common receptor models based on a weighted least squares fit (Paatero and Tapper, 1994). It is used to describe the variability of a multivariate dataset as the linear combination of a set of constant factor profiles and their corresponding time series as shown in Eq. (1) in cell notation:

$$x_{ij} = \sum_{k=1}^{p} g_{ik} f_{kj} + e_{ij} \, , \tag{1}$$

where **X**, **G**, **F** and **E** represent the data matrix, factor time series, factor profiles and residual matrices, respectively, while *i*, *j* and *k* indices denote time, element, and factor number. The index *p* represents the total number of factors in the PMF solution. The PMF model iteratively solves Eq. (1) by minimizing the object function (Q), defined as:

$$\mathrm{Q} = \sum_i \sum_j \left(\frac{e_{ij}}{s_{ij}}\right)^2 , \tag{2}$$

Here, s_{ij} corresponds to the measurement uncertainty (error matrix) for the input point *ij*.

The PMF algorithm was solved using ME-2 (Paatero, 1999) which enables an efficient exploration of the solution space by introducing *a priori* information to the **G** and / or **F** into the PMF model. Using the constraining technique of the *a*-value, one or more factor profile/factor time series can be confined by the scalar *a* ($0 \leq a \leq 1$) which can be applied to the entire profile/time series or to individual variables/data points of the profile/time series. The scalar *a* value defines how much the resolved factors are allowed to deviate from the input profile/time series, according to:

$$f'_{kj} = f_{kj} \pm a \times f_{kj} \, , \tag{3}$$

$$g'_{ik} = g_{ik} \pm a \times g_{ik} \, , \tag{4}$$

where the subscript *j* varies between 0 and the number of variables and *i* varies between 0 and the number of measured data points in time. f_{kj} and g_{ik} are the starting value used as a *priori* knowledge from base case solution in this SA study and f'_{kj} and g'_{ik} are the resulting values in the solution. Normalization in Eq. (3) and (4) can lead to the resulting values slightly outside the specified *a*-value boundaries. This method reduces the available solution space and directs the solution towards an optimized and environmentally meaningful solution. The Source Finder software SoFi Pro (v.6.2) (Canonaco et al., 2013) which is coded in Igor Pro software environment (Wavemetrics, Inc., Portland, OR, USA) was used for model configuration and analysis.

2.4 Conditional bivariate polar function (CBPF) plots

CBPF is a data analysis tool to find the direction of source contributions and was applied to the PMF source factors. Polar plots are used to present the CBPF analyses, where the number of events with a concentration greater than the 90th percentile is plotted as a function of both wind speed and direction, as shown in Eq. (5):

$$CBPF = \frac{m_{\theta,r}}{n_{\theta,r}}, \tag{5}$$

where $m_{\theta,r}$ is the number of samples in wind sector θ and wind speed sector r with a concentration greater than the 90th percentile and $n_{\theta,r}$ is the total number of samples with the same wind direction and speed (Carslaw and Beevers, 2013). The resultant CBPF polar plots present the probability that high concentrations of a pollutant correspond to a particular wind direction and speed and can give insight into the contributions from local and regional sources.

3 SA method and solutions selection

3.1 PMF input preparation

In our study, the PMF input consists of a data matrix and an error matrix of hourly trace element measurements where the rows represent the time series (456 points with 1 h steps) and the columns contain the trace elements (14 variables). The input preparation of PMF was done by excluding some specific trace elements for better source apportionment results. A common approach for the choice of species to include in the PMF input depends on the data below detection limit (Polissar et al., 1998). The minimum detection limits (MDL) for 1 h sampling of Xact trace elements are listed in Furger et al. (2017). The MDLs were given by the manufacturer and were calculated by using the sensitivity of the element and counts in the region of interest of a blank section of the tape from where 1σ interference-free detection limits are reported. Trace elements which had more than 50 % of data points below MDL were not included in the PMF input (e.g. V (98 %), Co (100 %), As (96 %), Se (62 %), Cd (87 %) and Pt (98 %), except Bi (93 %) which is a major tracer of fireworks and contains spikes during the fireworks episode. Some of the trace elements such as Ni, Hg, Sn and Sb were also excluded due to poor data quality. Missing data points in time (e.g. a power failure during sampling or a filter tape change) were removed from the data and error matrices. In the present work, if the trace element concentration was less than or equal to the MDL provided, the error matrix element s_{ij} was calculated using the Eq. (6) and if the concentration was greater than the MDL provided, the error matrix elementss_{ij} was calculated using Eq. (7) (Reff et al., 2007; Tian et al., 2016; Polissar et al., 1998):

$$s_{ij} = \frac{5}{6} \times MDL_j, \tag{6}$$

$$s_{ij} = \sqrt{(p_j \times x_{ij})^2 + (MDL_j)^2}\ , \qquad (7)$$

In this study, the p_j is the analytical uncertainty taken as 10 % for all of the chemical species.

3.2 PMF setup

An important step in the PMF analysis is the selection of the number of factors by the user, as mathematical diagnostics alone are insufficient for choosing the correct number of factors (Ulbrich et al., 2009; Canonaco et al., 2013). The selection of factors is often based on an analysis of the dependence of total Q or Q/Q_{exp}, scaled residuals (e_{ij}/s_{ij}), comparison of time series of the factor and external tracers, as well as diurnal patterns and the evaluation of the residual time series as a function of the number of resolved factors.

A preliminary source apportionment analysis was performed by unconstrained PMF (no *a priori* information on source fingerprints used) in order to determine the number of factors for the source apportionment analysis. The unconstrained PMF solutions yielded mixed factor solutions. Therefore, it was essential to constrain specific factor profiles and the time series in the PMF analysis to avoid mixing (see details in the Supplement, section S1, Fig. S1).

Residual analysis of the PMF runs showed obvious structure in the residuals for solutions having up to seven factors. Increasing the number of factors to eight gave evidence of structure removal, with mostly random errors remaining, while a further increase led to a new mixed factor of traffic-related and background dust which however had a noisy diurnal pattern (Figs. S1, S2, S3, S4). All the variables were approximately unimodal scaled residuals between ±3 (Paatero and Hopke, 2003) (Fig. S5).

3.3 Uncertainty estimate of PMF results

The statistical and rotational uncertainties were explored by the bootstrap (BS) resampling strategy (Efron, 1979) and the exploration of the *a*-value space of the constrained information as well as random initialization of the unconstrained information. Briefly, the bootstrap algorithm generates new input matrices by randomly resampling variables from the original input matrix. Each newly generated PMF input matrix had a total number of samples equal to the original matrix (456 samples); although some of the original 456 samples were represented several times, while others were not represented at all. A systematic investigation of the *a*-value space in combination with each individual BS runs is computationally impractical and was therefore replaced by random initialization of the *a*-value of the secondary sulfate, sea salt and fireworks-I factor profiles between 0 and 0.5 with an increment of 0.1 for 1000 BS runs. Moreover, to avoid rejection of many solutions due to mixing of the sea salt factor time series and the secondary sulfate time series with the fireworks factor peaks, both the sea salt and secondary factor time series were also constrained with *a*-value 0.01. Solutions were selected and retained based on the correlation (Pearson *R*) of the time series between the factors of the base case and the factors of the BS runs. Solutions with low correlation and some solutions with high correlation have a factor of completely different type i.e. mixed or split or otherwise altered factor profile/time series based on visual inspection. These kinds of solutions were rejected. This approach is used only for uncertainty assessment rather than uncertainty exploration to find the environmentally reasonable solution.

We also performed separate random bootstrap analyses for 1000 times on the correlation (Pearson *R*) between the time series of a base case factor and the respective external marker, e.g. the secondary sulfate factor vs ACSM sulfate, and the traffic-related factor vs NO_x to assess the acceptable uncertainty of the Pearson-*R* correlation value. The resulting Pearson correlation coefficients were represented in probability density functions (PDF) over 1000 bootstrap runs for both bootstrap analysis methods. In total 86% bootstrap runs were classified as environmentally good solutions. The average *a*-value retained by the selected bootstrap runs was 0.233, 0.255 and 0.241 for fireworks-I, sea salt and secondary sulfate factor profiles, respectively. The spread of *a*-value for these three factors is presented as mean, median and interquartile in the supplement (Fig. S6). The selected solutions factor profiles are represented as box whisker plot in the sequence of p10 (10th percentile), p25 (25th percentile), p50 or median (50th percentile), p75 (75th percentile) and p90 (90th percentile) in Fig. 1.

4 Results and discussion

4.1 Overview of retrieved factors

The solution that best represented the input data was the eight-factor solution. The eight factors from the PMF results are as follows:

1. Two fireworks factors with prominent relative contributions of Bi, Ba, K, S, Ti, Cu and Cl, which are important components of fireworks (Kong et al., 2015; Vecchi et al., 2008);
2. A sea salt factor explaining a large fraction of Cl in the coarse fraction;
3. A secondary sulfate factor mostly dominated by S and highly correlated with ACSM sulfate; (Fig. S7);
4. Two dust factors, one dominated by Ca and showing traffic rush hours peaks and the other dominated by Si without clear diurnal pattern;
5. A traffic-related factor characterized by Fe, Cr, Cu, Mn, Zn and Ba;
6. An industrial factor showing relatively high contributions of Pb and Zn.

4.2 Detailed factor description

In this section the final results of the PM_{10} source apportionment are presented and validated. Fig. 1 represents the factor composition ($f_{kj}/\sum_j f_{kj}$) (left y-axis; colored box whisker plots for each factor) and relative contribution ($\sum_i g_{ik} f_{kj}/\sum_k \sum_i g_{ik} f_{kj}$) of each factor to each variable (right y-axis; black box whisker plots). Fig. 2a shows the time series of the absolute mass (bottom panels) and relative contributions (top panel) of the retrieved PM_{10} factors. The variability of these time series across all good solutions was relatively low. Fig. 2b reports the averaged total PM_{10} elemental mass (excluding the fireworks factors) and relative contributions of the PM_{10} elemental sources. The reported variabilities/uncertainties (which correspond to the interquartile range among selected bootstrap runs) are an indication of the high stability of the solution. The daily patterns of the absolute concentrations of the identified factors and some of their corresponding external tracers are presented in Fig. 3. CBPF analysis was performed to validate some of the identified sources and their characterization (Fig. S8).

Fireworks: The fireworks factor profiles and time series are shown in Fig. 1 and Fig. 2a respectively. The fireworks factors are mostly dominated by K, S, Cl, Ti, Cu, Ba and Bi, which are the main chemical elemental species of fireworks. Ba and Cu compounds are used to produce green and blue fireworks. The presence of Cl in fireworks-I suggests that the chloride salt might be the main chemical form in the fireworks, such as barium chloride. K is one of the major components of fireworks, which contain 74 % of KNO_3 in black powder as the oxidizing agent for the burning process (Drewnick et al., 2006). The K / S ratio of 2.72 in the fireworks-I factor profile is in good agreement with the K / S elemental concentration ratio (~2.76) in black powder (Dutcher et al., 1999). Other K compounds in black powder can be in the form of perchlorate or chlorate (Wang et al., 2007). Bi is used to produce crackling sounds in fireworks. The Ba / K ratio of 0.031-0.054 for fireworks-I and fireworks-II is close to the value 0.057 reported in (Pongpiachan et al., 2018). Fireworks particles are usually present in large amounts in the fine fraction, staying longer in the atmosphere (Richard et al., 2011; Moreno et al., 2007).

The diurnal patterns of these elements exhibit a peak at 23:00 LT (or CEST) during the fireworks period (Furger et al., 2017) in accordance with the fireworks-I diurnal variation (Fig. 3c). A pronounced increase in both fireworks factor time series is observed when the fireworks traditionally begin. Both fireworks factors contain two sharp peaks. The fireworks-I factor concentration started to increase on 31 July 2015 22:00 LT and formed the extreme peak within 1 h at 23:00 LT (~5 $\mu g\ m^{-3}$). After that it decayed quickly (10 times lower concentration than maximum fireworks concentration) within 1 h and remained more or less constant until 1 August 2015 21:00 LT. It again started to increase from 22:00 LT and formed a second sharp peak on 1 August 2015 23:00 LT, followed by a gradual decay over the next 6 to 10 h. Fireworks-II presents a slightly different pattern in its time series. It started to increase from 31 July 2015 22:00 LT and depicted its highest peak at 00:00 LT (~3.6 $\mu g\ m^{-3}$) with a quite slow decay until 1 August 2015 06:00 LT. The concentration remained slightly higher than fireworks-I over daytime. It then started to increase again from 1 August 2015 17:00 LT and yielded the highest peak on 2 August 04:00 LT with 6.7 $\mu g\ m^{-3}$. It remained higher until 2 August 2015 08:00 LT and slowly decayed until the afternoon, followed by further prominent peaks at 23:00 LT on 2 August and 3 August. The time series variations in both fireworks suggest that fireworks-I might be related to the main fireworks celebration while fireworks-II might result from burning of leftover crackers after the main fireworks day, as well as the influence of other sources such as bonfires, which are a common activity during Swiss National Day celebrations. Another possibility could be the advection of fireworks clouds from nearby cities where grand firework displays and bonfires are carried out at large scale to celebrate the Swiss National Day. The aging induced by reactions of KCl with acids like HNO_3 may cause the absence of particulate Cl by release of HCl. This could explain the absence of Cl in the fireworks-II factor profile. The average relative contributions of fireworks-I and fireworks-II to the analysed mass were 7.4 % and 11 % respectively (Fig. 2b).

Fig. 4 represents the fireworks data points for each element. A K concentration > 220 ng m^{-3} was used as the criterion to separate fireworks data points (65 data points) from the whole data set. The mean values (with one standard deviation) of the elements normalized by the averaged values of the total fireworks concentration are presented as box-whisker plots (fireworks-I factor composition as red dots and fireworks-II factor composition as green dots). This figure highlights the fact that most of the elements are well captured by two fireworks factors such as S, K, Fe, Cu, Ba etc. since they lie within the fireworks data distribution. There are some elements that are not contributing to fireworks e.g. Ca and Cr while some elements are explained by only one firework, e.g., Si, Cl and Pb. This indicates that a single fireworks factor is not enough to represent the fireworks data variability.

Sea salt: The sea salt factor was mainly composed of Cl (81 % of total factor composition) as shown in the factor profile (Fig. 1), with no diurnal pattern (Fig. 3e). The average relative contribution of the sea salt factor to the analysed mass was 3.7 % (Fig. 2b). Sea salt also includes Na and Mg, which were not measured by the Xact. Based on the high correlation of Na and Cl in a previous study, Cl alone can be used as a marker for sea salt particles (Vallius, 2005). The existence of sea salt particles was confirmed by a low Mg / Na ratio in the 24-h filter data, for days with Cl concentration, with Mg / Na equalling 0.13 and 0.16 for 28 July and 30 July, respectively, in line with a ratio of 0.132 to 0.185 for marine aerosol (Chesselet et al., 1972). For the remaining 8 filter samples Mg / Na was higher than 0.18, probably due to absence of sea salt (Fig. S9). A comparison with ACSM data revealed that Cl was mainly present in the fine fraction during firework days and mainly in the coarse mode otherwise (Fig. S10). In addition, the highest Cl concentrations were observed only in the last week of July, with westerly winds at higher wind speed (5–8 m s^{-1}) (Fig. S10, S11). This result is in agreement with the CBPF plot where the high concentration of the sea salt factor dominates for westerly winds with high wind speed (Fig. S8) and confirms previous studies (Visser et al., 2015; Twigg et al., 2015).

Dust: PMF analysis resolved two dust-related factors, i.e., a road dust (Ca-rich) and a background dust (Si-rich) factor, with average relative contributions to the analysed mass of 18 % and 16 %, respectively (Fig. 2b). The road dust factor was mainly composed of Ca (68 % of total factor composition) followed by Si (26 %) with relative contributions of 89 % to Ca, 19 % to Si and 12 % to Mn; while the background dust factor highly contributed to Ti, Si, Mn, Fe and Ca, with 65 %, 58 %, 22 %, 16 % and 6 %, respectively. The two dust factors together explain 95 % of Ca, with no other factor explaining more than 93 %. The solution with two dust factors resulted in reduced scaled residuals for Si and Ca compared to a solution with one dust factor (Fig. S12). The scatter plot between the absolute concentrations of Si and Ca also indicates the presence of two different sources (Fig. S13). The high relative contribution of Ca in road dust has been seen in other source apportionment studies also (Ducret-Stich et al., 2013; Bukowiecki et al., 2010). In general, Ca is commonly associated with mineral dust, construction activities, vehicular emissions and iron/steel plants. Iron/steel plants produce furnace slacks; a glass-like by-product which consists of Ca, Si, Mg and Al oxides. The higher fraction of crustal elements such as Ca and Si in road dust might be a consequence of the widespread use of asphalt/concrete to make roads (Fullova et al., 2017; Li et al., 2004). The sampling site is located close to the freeway and may be influenced by wear and tear of the asphalt/concrete roads because of heavy traffic. The background dust factor profile exhibits elements associated with mineral dust such as Ti, Si and Fe. These and other terrestrial elements are commonly present in soil as oxides (Rudnick and Gao, 2003).

The background dust factor also contains a significant fraction of the measured Mn, which is one of the most abundant compounds in the earth's crust, where it occurs in the form of MnO_2 (Taylor and McLennan, 1995). Since the sampling site is surrounded by agricultural fields, the contribution of these elements to this factor can be expected. A similar background factor with high contributions of Si, Ti and Ca was found by Richard et al. (2011) at an urban site in Switzerland.

The separation of two dust factors is in line with Amato et al. (2009) where ME-2 yielded a road dust factor distinct from a mineral dust factor. The CBPF plots shows that higher concentrations of the road dust factor are associated with the southern wind sector, while the background dust factor is influenced by the southwest wind sector with a small tail in the north sector (Fig. S8). The diurnal pattern of the road dust factor shows morning rush hour traffic peaks similar to NO_x, black carbon (BC), heavy duty vehicle (HDV) count and traffic-related factor (Fig. 3a, 3b) indicating resuspension of road dust is due to the vehicle fleet. A similar relationship between road dust and the traffic-related source was observed in a previous study (Amato et al., 2009). Resuspension of road dust in the early morning traffic is not triggered by wind speed (Fig. S14) but by the traffic fleet, whereas in the afternoon, an increase in wind speed leads to resuspension of dust deposited on the road as well as resuspension of agricultural soil dust at the sampling site. Therefore, meteorology plays a vital role for the contribution of the background dust factor.

Traffic-related: The traffic-related factor composition was mostly dominated by Fe (73 % of total factor composition) and contributed strongly to Cr (96 %), Fe (76 %), Cu (71 %), Mn (50 %), Zn (31 %), Ba (26 %) and Si (12 %). Its average relative contribution to the analysed mass was 20 % (Fig. 2b). Coarse particles from brake/disc wear could appear as flakes and mainly consist of iron oxides (Wahlström et al., 2010). The higher fraction of Fe in the traffic-related source has been found in several previous studies (Visser et al., 2015; Amato et al., 2014a; Bukowiecki et al., 2010; Dall'Osto et al., 2013; Crilley et al., 2016). However, the ratio of Fe to other elements is variable between studies. Fe, Cr, Cu, Zn, Mn and Ba are the most abundant trace elements in brake pads, brake lining and thus attributed to tire/brake wear (Thorpe and Harrison, 2008; Grigoratos and Martini, 2015; Gianini et al., 2012) and engine wear. This factor is characterized by a strong diurnal peak coinciding with the morning rush hour at 08:00 LT, similar to NO_x and BC (Fig. 3b). The light duty vehicle (LDV) and HDV counts start to increase from 05:00 LT (Fig. 3a), unlike the primary traffic emission NO_x and BC. The similar diurnal pattern of this factor might be due to the high braking load for vehicles during peak traffic hours, resulting in increased emissions of vehicle wear particles.

Secondary sulfate: This source is characterized by sulfur (S) and is most likely due to the regional background contribution of secondary sulfate due to conversion of SO_2 to SO_4^{2-}, consistent with the results of many previous source apportionment studies (Dall'Osto et al., 2013; Richard et al., 2011). It explains the highest fraction of S (91 % of total factor composition) with relative contributions to S (73%) and Pb (30%) (Fig. 1). The average relative contribution of this factor is 21 % of the analysed mass (Fig. 2b). Similar factor profiles were found in previous studies (Visser et al., 2015; Dall'Osto et al., 2013). This factor correlates well with ACSM SO_4^{2-} measurements (Pearson's R 0.91), suggesting a dominant contribution from the submicron fraction and thus a slow rate of dry deposition. Combined with SO_2 oxidation processes occurring on timescales hours to days, it is thus reasonable that the secondary sulfate factor does not exhibit a clear diurnal variation (Fig. 3f) and is consistent with regional rather than local sources. The time series of secondary sulfate exhibits peaks during the fireworks event (Fig. 2a), in agreement with the ACSM SO_4^{2-} time series (Fig. S12). The secondary sulfate factor and the ACSM SO_4^{2-} capture the highest peak at midnight on 2 August 2015, while fireworks-I formed a peak at 23:00 LT on 1 August 2015. The time series of ACSM SO_4^{2-} and ACSM NH_4^+ show significant correlation (Fig. S12), indicating the formation of ammonium sulfate particles except for the main fireworks peaks.

Industrial: This factor is characterized by high relative contributions to Zn (50 %) and Pb (63 %), with a low contribution to the analysed mass (in the order of 3 %, Fig. 2b). A similar factor profile was observed in previous source apportionment studies (Crilley et al., 2016; Dall'Osto et al., 2013; Richard et al., 2011; Vossler et al., 2016; Amato et al., 2010). The profile is shown in Fig. 1 and time series in Fig. 2a. The time series contains a few spikes after 4 August when the wind was predominantly from the south and south-east sector, suggesting industrial emissions. Industrial emissions play a rather small role in this study area as it is surrounded by only a few small scale industrial buildings (logistics businesses approximately 500 m to the north-west and a wheel manufacturing company to the south-east across the freeway). The CPBF plot confirms the dominance of high concentrations in south-east direction (Fig. S8). The diurnal cycle demonstrated a clear peak at 10:00 LT (Fig. 3g) which however may be coincidental, as it is related to a few peaks.

5 Conclusion

A source apportionment study of elements in PM_{10} measured at a traffic-influenced site in Härkingen, Switzerland; during summer 2015 was conducted using the ME-2 implementation of PMF. The PMF model was able to resolve and evaluate the contributions and compositions of eight sources: two fireworks factors, sea salt, secondary sulfate, background dust, road dust, traffic-related, and an industrial source. The use of ME-2 allowed the use of constraints via the *a*-value approach, which improved factor resolution relative to conventional PMF. We established that data sets including extreme events such as fireworks can be apportioned by ME-2 without disturbing the model solutions. This was only achievable when controlling problematic factors, i.e., factors that tend to mix within the constraining technique. Two dust factors with different time profiles and two fireworks factors were identified by the PMF model resulting in better representation of data variability. A S-rich (secondary sulfate) factor which can typically be attributed to regional background/transported secondary sulfate was correlated with fine mode non-refractory sulfate measured by an ACSM. The traffic-related factor followed the diurnal patterns of traffic rush hours similar to NO_x and BC with concentrations up to 4 times higher during daytime relative to night-time. This result emphasizes the large influence of highway traffic on the composition of PM_{10}. The small contribution of the industrial factor confirms the low influence of local daily activities from the surroundings.

It was shown that high time resolution trace elements data sets enable a fully resolved SA, with considerable improvements compared to 24-h filter analysis, where the attribution to specific sources is possible only on a larger time scale and is mostly based on seasonal variations.

Data availability

The datasets are available upon request to the corresponding author.

Author contribution

PR performed SA analysis and wrote the manuscript. MF, RF and CH performed measurement. MF and RF analysed data for Xact and ACSM, respectively. FC provided expertise on software for SA analysis. MCM provided ICP-MS and ICP-AES analysis data. KP lent Xact® 625 for measurement. UB, ASHP, MF, FC and JS were involved with the supervision and conceptualisation. All authors commented on the paper and assisted in the interpretation of the results.

Competing interests

Krag Petterson is employed by Cooper Environmental Services, the manufacturer of the Xact® 625.

Acknowledgements

This study has been funded by Swiss National Science Foundation (SNSF grant: 200021_162448/1 and BSSGI0_155846) and by the Swiss Federal Office for the Environment (FOEN). We thank René Richter and Roland Scheidegger of PSI for their technical support during the measurement campaign. We are grateful to Chris Koch and Varun Yadav of Cooper Environmental Services for instructions on instrument. We thank the operators of the NABEL stations for providing all supports during measurement.

References

Amato, F., Pandolfi, M., Escrig, A., Querol, X., Alastuey, A., Pey, J., Perez, N., and Hopke, P. K.: Quantifying road dust resuspension in urban environment by Multilinear Engine: A comparison with PMF2, Atmos. Environ., 43, 2770–2780, https://doi.org/10.1016/j.atmosenv.2009.02.039, 2009.

Amato, F., Nava, S., Lucarelli, F., Querol, X., Alastuey, A., Baldasano, J. M., and Pandolfi, M.: A comprehensive assessment of PM emissions from paved roads: Real-world emission factors and intense street cleaning trials, Sci. Total Environ., 408, 4309–4318, https://doi.org/10.1016/j.scitotenv.2010.06.008, 2010.

Amato, F., Pandolfi, M., Moreno, T., Furger, M., Pey, J., Alastuey, A., Bukowiecki, N., Prevot, A. S. H., Baltensperger, U., and Querol, X.: Sources and variability of inhalable road dust particles in three European cities, Atmos. Environ., 45, 6777–6787, https://doi.org/10.1016/j.atmosenv.2011.06.003, 2011.

Amato, F., Alastuey, A., de la Rosa, J., Sánchez de la Campa, A. M., Pandolfi, M., Lozano, A., Contreras González, J., and Querol, X.: Trends of road dust emissions contributions on ambient air particulate levels at rural, urban and industrial sites in southern Spain, Atmos. Chem. Phys., 14, 3533–3544, https://doi.org/10.5194/acp-14-3533-2014, 2014a.

Amato, F., Cassee, F. R., Denier van der Gon, H. A. C., Gehrig, R., Gustafsson, M., Hafner, W., Harrison, R. M., Jozwicka, M., Kelly, F. J., Moreno, T., Prevot, A. S. H., Schaap, M., Sunyer, J., and Querol, X.: Urban air quality: The challenge of traffic non-exhaust emissions, J. Hazard. Mater., 275, 31–36, https://doi.org/10.1016/j.jhazmat.2014.04.053, 2014b.

Ancelet, T., Davy, P. K., Mitchell, T., Trompetter, W. J., Markwitz, A., and Weatherburn, D. C.: Identification of particulate matter sources on an hourly time-scale in a wood burning community, Environ. Sci. Technol., 46, 4767–4774, https://doi.org/10.1021/es203937y, 2012.

Bozzetti, C., Daellenbach, K. R., Hueglin, C., Fermo, P., Sciare, J., Kasper-Giebl, A., Mazar, Y., Abbaszade, G., El Kazzi, M., Gonzalez, R., Shuster-Meiseles, T., Flasch, M., Wolf, R., Křepelová, A., Canonaco, F., Schnelle-Kreis, J., Slowik, J. G., Zimmermann, R., Rudich, Y., Baltensperger, U., El Haddad, I., and Prévôt, A. S. H.: Size-resolved identification, characterization, and quantification of primary biological organic aerosol at a European rural site, Environ. Sci. Technol., 50, 3425–3434, https://doi.org/10.1021/acs.est.5b05960, 2016.

Brauer, M., Hoek, G., Vliet, P. V., Meliefste, K., Fischer, P. H., Wijga, A., Koopman, L. P., Neijens, H. J., Gerritsen, J., Kerkhof, M., Heinrich, J., Bellander, T., and Brunekreef, B.: Air pollution from traffic and the development of respiratory infections and asthmatic and allergic symptoms in children, Am. J. Respir. Crit. Care Med., 166, 1092–1098, https://doi.org/10.1164/rccm.200108-007OC, 2002.

Bukowiecki, N., Lienemann, P., Zwicky, C. N., Furger, M., Richard, A., Falkenberg, G., Rickers, K., Grolimund, D., Borca, C., Hill, M., Gehrig, R., and Baltensperger, U.: X-ray fluorescence spectrometry for high throughput analysis of atmospheric aerosol samples: The benefits of synchrotron X-rays, Spectrochim. Acta B, 63, 929–938, https://doi.org/10.1016/j.sab.2008.05.006, 2008.

Bukowiecki, N., Lienemann, P., Hill, M., Figi, R., Richard, A., Furger, M., Rickers, K., Falkenberg, G., Zhao, Y., Cliff, S. S., Prévôt, A. S. H., Baltensperger, U., Buchmann, B., and Gehrig, R.: Real-world emission factors for antimony and other brake wear related trace elements: size-segregated values for light and heavy duty vehicles, Environ. Sci. Technol., 43, 8072–8078, https://doi.org/10.1021/es9006096, 2009.

Bukowiecki, N., Lienemann, P., Hill, M., Furger, M., Richard, A., Amato, F., Prévôt, A. S. H., Baltensperger, U., Buchmann, B., and Gehrig, R.: PM_{10} emission factors for non-exhaust particles generated by road traffic in an urban street canyon and along a freeway in Switzerland, Atmos. Environ., 44, 2330–2340, https://doi.org/10.1016/j.atmosenv.2010.03.039, 2010.

Cakmak, S., Dales, R., Kauri, L. M., Mahmud, M., Ryswyk, K. V., Vanos, J., Liu, L., Kumarathasan, P., Thomson, E., Vincent, R., and Weichenthal, S.: Metal composition of fine particulate air pollution and acute changes in cardiorespiratory physiology, Environ. Pollut., 189, 208–214, https://doi.org/10.1016/j.envpol.2014.03.004, 2014.

Canonaco, F., Crippa, M., Slowik, J. G., Baltensperger, U., and Prévôt, A. S. H.: SoFi, an IGOR-based interface for the efficient use of the generalized multilinear engine (ME-2) for the source apportionment: ME-2 application to aerosol mass spectrometer data, Atmos. Meas. Tech., 6, 3649–3661, https://doi.org/10.5194/amt-6-3649-2013, 2013.

Carslaw, D. C. and Beevers, S. D.: Characterising and understanding emission sources using bivariate polar plots and k-means clustering, Environ. Modell. Softw., 40, 325–329, https://doi.org/10.1016/j.envsoft.2012.09.005, 2013.

Cesari, D., Genga, A., Ielpo, P., Siciliano, M., Mascolo, G., Grasso, F. M., and Contini, D.: Source apportionment of $PM_{2.5}$ in the harbour-industrial area of Brindisi (Italy): Identification and estimation of the contribution of in-port ship emissions, Sci. Total Environ., 497–498, 392–400, https://doi.org/10.1016/j.scitotenv.2014.08.007, 2014.

Chang, Y., Huang, K., Xie, M., Deng, C., Zou, Z., Liu, S., and Zhang, Y.: First long-term and near real-time measurement of trace elements in China's urban atmosphere: temporal variability, source apportionment and precipitation effect, Atmos. Chem. Phys., 18, 11793–11812, https://doi.org/10.5194/acp-18-11793-2018, 2018.

Chesselet, R., Morelli, J., and Buat-Menard, P.: Variations in ionic ratios between reference sea water and marine aerosols, J. Geophys. Res., 77, 5116–5131, https://doi.org/10.1029/JC077i027p05116, 1972.

Crenn, V., Sciare, J., Croteau, P. L., Verlhac, S., Fröhlich, R., Belis, C. A., Aas, W., Äijälä, M., Alastuey, A., Artiñano, B., Baisnée, D., Bonnaire, N., Bressi, M., Canagaratna, M., Canonaco, F., Carbone, C., Cavalli, F., Coz, E., Cubison, M. J., Esser-Gietl, J. K., Green, D. C., Gros, V., Heikkinen, L., Herrmann, H., Lunder, C., Minguillón, M. C., Močnik, G., O'Dowd, C. D., Ovadnevaite, J., Petit, J.-E., Petralia, E., Poulain, L., Priestman, M., Riffault, V., Ripoll, A., Sarda-Estève, R., Slowik, J. G., Setyan, A., Wiedensohler, A., Baltensperger, U., Prévôt, A. S. H., Jayne, J. T., and Favez, O.: ACTRIS ACSM intercomparison – Part 1: Reproducibility of concentration and fragment results from 13 individual Quadrupole Aerosol Chemical Speciation Monitors (Q-ACSM) and consistency with co-located instruments, Atmos. Meas. Tech., 8, 5063–5087, https://doi.org/10.5194/amt-8-5063-2015, 2015.

Crilley, L. R., Lucarelli, F., Bloss, W. J., Harrison, R. M., Beddows, D. C., Calzolai, G., Nava, S., Valli, G., Bernardoni, V., and Vecchi, R.: Source apportionment of fine and coarse particles at a roadside and urban background site in London during the 2012 summer ClearfLo campaign, Environ. Pollut., 220, 766–778, https://doi.org/10.1016/j.envpol.2016.06.002, 2016.

Dall'Osto, M., Querol, X., Amato, F., Karanasiou, A., Lucarelli, F., Nava, S., Calzolai, G., and Chiari, M.: Hourly elemental concentrations in $PM_{2.5}$ aerosols sampled simultaneously at urban background and road site during SAPUSS – diurnal variations and PMF receptor modelling, Atmos. Chem. Phys., 13, 4375–4392, https://doi.org/10.5194/acp-13-4375-2013, 2013.

Dao, L., Morrison, L., and Zhang, C.: Bonfires as a potential source of metal pollutants in urban soils, Galway, Ireland, Appl. Geochem., 27, 930–935, https://doi.org/10.1016/j.apgeochem.2012.01.010, 2012.

Dockery, D. W., Pope III, C. A., Xu, X., Spengler, J. D., Ware, J. H., Fay, M. E., Ferris, B. G., and Speizer, F. E.: An association between air pollution and mortality in six U.S. cities, The New England J. Med., 329, 1753–1759, 1993.

Drewnick, F., Hings, S. S., Curtius, J., Eerdekens, G., and Williams, J.: Measurement of fine particulate and gas-phase species during the New Year's fireworks 2005 in Mainz, Germany, Atmos. Environ., 40, 4316–4327, https://doi.org/10.1016/j.atmosenv.2006.03.040, 2006.

Ducret-Stich, R. E., Tsai, M.-Y., Thimmaiah, D., Kunzli, N., Hopke, P. K., and Phuleria, H. C.: PM_{10} source apportionment in a Swiss Alpine valley impacted by highway traffic, Environ. Sci. Pollut. Res., 20, 6496–6508, https://doi.org/10.1007/s11356-013-1682-1, 2013.

Dutcher, D. D., Perry, K. D., Cahill, T. A., and Copeland, S. A.: Effects of indoor pyrotechnic displays on the air quality in the Houston Astrodome, J. Air Waste Manage. Assoc., 49, 156–160, https://doi.org/10.1080/10473289.1999.10463790, 1999.

Efron, B.: Bootstrap methods: Another look at the Jacknife, The Ann. Stat., 7, 1–26, 1979.

Fullova, D., Durcanska, D., and Hegrova, J.: Particulate matter mass concentrations produced from pavement surface abrasion, MATEC Web of Conferences, 117, 00048, https://doi.org/10.1051/matecconf/201711700048, 2017.

Furger, M., Minguillón, M. C., Yadav, V., Slowik, J. G., Hüglin, C., Fröhlich, R., Petterson, K., Baltensperger, U., and Prévôt, A. S. H.: Elemental composition of ambient aerosols measured with high temporal resolution using an online XRF spectrometer, Atmos. Meas.Tech., 10, 2061–2076, https://doi.org/10.5194/amt-10-2061-2017, 2017.

Gianini, M. F. D., Fischer, A., Gehrig, R., Ulrich, A., Wichser, A., Piot, C., Besombes, J.-L., and Hueglin, C.: Comparative source apportionment of PM_{10} in Switzerland for 2008/2009 and 1998/1999 by positive matrix factorisation, Atmos. Environ., 54, 149–158, https://doi.org/10.1016/j.atmosenv.2012.02.036, 2012.

Grigoratos, T. and Martini, G.: Brake wear particle emissions: a review, Environ. Sci. Pollut. Res., 22, 2491–2504, https://doi.org/10.1007/s11356-014-3696-8, 2015.

Harrison, R. M., Beddows, D. C. S., and Dall'Osto, M.: PMF analysis of wide-range particle size spectra collected on a major highway, Environ. Sci. Technol., 45, 5522–5528, https://doi.org/10.1021/es2006622, 2011.

Hedberg, E., Gidhagen, L., and Johansson, C.: Source contributions to PM_{10} and arsenic concentrations in Central Chile using positive matrix factorization, Atmos. Environ., 39, 549–561, https://doi.org/10.1016/j.atmosenv.2004.11.001, 2005.

Hueglin, C., Buchmann, B., and Weber, R. O.: Long-term observation of real-world road traffic emission factors on a motorway in Switzerland, Atmos. Environ., 40, 3696–3709, https://doi.org/10.1016/j.atmosenv.2006.03.020, 2006.

Jeong, C.-H., Wang, J. M., Hilker, N., Debosz, J., Sofowote, U., Su, Y., Noble, M., Healy, R. M., Munoz, T., Dabek-Zlotorzynska, E., Celo, V., White, L., Audette, C., Herod, D., and Evans, G. J.: Temporal and spatial variability of traffic-related $PM_{2.5}$ sources: Comparison of exhaust and non-exhaust emissions, Atmos. Environ., 198, 55–69, https://doi.org/10.1016/j.atmosenv.2018.10.038, 2019.

Kelly, F. J. and Fussell, J. C.: Air pollution and airway disease, Clin. Exp. Allergy, 41, 1059–1071, https://doi.org/10.1111/j.1365-2222.2011.03776.x, 2011.

Kelly, F. J. and Fussell, J. C.: Size, source and chemical composition as determinants of toxicity attributable to ambient particulate matter, Atmos. Environ., 60, 504–526, https://doi.org/10.1016/j.atmosenv.2012.06.039, 2012.

Kidwell, C. B. and Ondov, J. M.: Development and evaluation of a prototype system for collecting sub-hourly ambient aerosol for chemical analysis, Aerosol Sci. Tech., 35, 596–601, https://doi.org/10.1080/02786820118049, 2001.

Kim, E., Hopke, P. K., and Edgerton, E. S.: Source identification of Atlanta aerosol by positive matrix factorization, J. Air Waste Manage. Assoc., 53, 731–739, https://doi.org/10.1080/10473289.2003.10466209, 2003.

Kong, S. F., Li, L., Li, X. X., Yin, Y., Chen, K., Liu, D. T., Yuan, L., Zhang, Y. J., Shan, Y. P., and Ji, Y. Q.: The impacts of firework burning at the Chinese Spring Festival on air quality: insights of tracers, source evolution and aging processes, Atmos. Chem. Phys., 15, 2167–2184, https://doi.org/10.5194/acp-15-2167-2015, 2015.

Lanz, V. A., Prévôt, A. S. H., Alfarra, M. R., Weimer, S., Mohr, C., DeCarlo, P. F., Gianini, M. F. D., Hueglin, C., Schneider, J., Favez, O., D'Anna, B., George, C., and Baltensperger, U.: Characterization of aerosol chemical composition with aerosol mass spectrometry in Central Europe: an overview, Atmos. Chem. Phys., 10, 10453–10471, https://doi.org/10.5194/acp-10-10453-2010, 2010.

Lawrence, S., Sokhi, R., Ravindra, K., Mao, H., Prain, H. D., and Bull, I. D.: Source apportionment of traffic emissions of particulate matter using tunnel measurements, Atmos. Environ., 77, 548–557, https://doi.org/10.1016/j.atmosenv.2013.03.040, 2013.

Li, Z., Hopke, P. K., Husain, L., Qureshi, S., Dutkiewicz, V. A., Schwab, J. J., Drewnick, F., and Demerjian, K. L.: Sources of fine particle composition in New York city, Atmos. Environ., 38, 6521–6529, https://doi.org/10.1016/j.atmosenv.2004.08.040, 2004.

Lin, Y.-C., Tsai, C.-J., Wu, Y.-C., Zhang, R., Chi, K.-H., Huang, Y.-T., Lin, S.-H., and Hsu, S.-C.: Characteristics of trace metals in traffic-derived particles in Hsuehshan Tunnel, Taiwan: size distribution, potential source, and fingerprinting metal ratio, Atmos. Chem. Phys., 15, 4117–4130, https://doi.org/10.5194/acp-15-4117-2015, 2015.

Lucarelli, F., Nava, S., Calzolai, G., Chiari, M., Udisti, R., and Marino, F.: Is PIXE still a useful technique for the analysis of atmospheric aerosols? The LABEC experience, X-Ray Spectrom., 40, 162–167, https://doi.org/10.1002/xrs.1312, 2011.

Manousakas, M., Diapouli, E., Papaefthymiou, H., Migliori, A., Karydas, A. G., Padilla-Alvarez, R., Bogovac, M., Kaiser, R. B., Jaksic, M., Bogdanovic-Radovic, I., and Eleftheriadis, K.: Source apportionment by PMF on elemental concentrations obtained by PIXE analysis of PM_{10} samples collected at the vicinity of lignite power plants and mines in Megalopolis, Greece, Nucl. Instr. Meth. Phys. Res. Sec. B, 349, 114–124, https://doi.org/10.1016/j.nimb.2015.02.037, 2015.

Minguillon, M. C., Querol, X., Baltensperger, U., and Prévôt, A. S. H.: Fine and coarse PM composition and sources in rural and urban sites in Switzerland: local or regional pollution?, Sci. Total Environ., 427–428, 191–202, https://doi.org/10.1016/j.scitotenv.2012.04.030, 2012.

Moreno, T., Querol, X., Alastuey, A., Minguillón, M. C., Pey, J., Rodriguez, S., Miró, J. V., Felis, C., and Gibbons, W.: Recreational atmospheric pollution episodes: Inhalable metalliferous particles from firework displays, Atmos. Environ., 41, 913–922, https://doi.org/10.1016/j.atmosenv.2006.09.019, 2007.

Ng, N. L., Herndon, S. C., Trimborn, A., Canagaratna, M. R., Croteau, P. L., Onasch, T. B., Sueper, D., Worsnop, D. R., Zhang, Q., Sun, Y. L., and Jayne, J. T.: An aerosol chemical speciation monitor (ACSM) for routine monitoring of the composition and mass concentrations of ambient aerosol, Aerosol Sci. Tech., 45, 780–794, https://doi.org/10.1080/02786826.2011.560211, 2011.

Norris, G., Duvall, R., Brown, S., and Bai, S.: EPA Positive Matrix Factorization (PMF) 5.0 fundamentals and user guide prepared for the United States Environmental Protection Agency Office of Reseach and Development, Washington DC, 2014.

Paatero, P.: The Multilinear Engine – A table-driven, least squares program for solving multilinear problems, including the n-way parallel factor analysis model, J. Comput. Graph. Stat., 8, 854–888, https://doi.org/10.1080/10618600.1999.10474853-1999, 1999.

Paatero, P. and Hopke, P. K.: Discarding or downweighting high-noise variables in factor analytic models, Anal. Chim. Acta, 490, 277–289, https://doi.org/10.1016/s0003-2670(02)01643-4, 2003.

Paatero, P. and Tapper, U.: Positive matrix factorization: A non-negative factor model with optimal utilization of error-estimates of data values, Environmetrics, 5, 111–126, https://doi.org/10.1002/env.3170050203, 1994.

Park, S. S., Cho, S. Y., Jo, M. R., Gong, B. J., Park, J. S., and Lee, S. J.: Field evaluation of a near-real time elemental monitor and identification of element sources observed at an air monitoring supersite in Korea, Atmos. Poll. Res., 5, 119–128, https://doi.org/10.5094/apr.2014.015-2014, 2014.

Polissar, A. V., Hopke, P. K., Paatero, P., Malm, W. C., and Sisler, J. F.: Atmospheric aerosol over Alaska: 2. Elemental composition and sources, J. Geophys. Res., 103, 19045–19057, https://doi.org/10.1029/98JD01212, 1998.

Pongpiachan, S., Iijima, A., and Cao, J.: Hazard quotients, hazard indexes, and cancer risks of toxic metals in PM_{10} during firework displays, Atmosphere, 9, 144, https://doi.org/10.3390/atmos9040144, 2018.

Pope III, C. A. and Dockery, D. W.: Health effects of fine particulate air pollution: Lines that connect, J. Air Waste Manage. Assoc., 56, 709–742, https://doi.org/10.1080/10473289.2006.10464485, 2006.

Rahman, S. A., Hamzah, M. S., Wood, A. K., Elias, M. S., Salim, N. A. A., and Sanuri, E.: Sources apportionment of fine and coarse aerosol in Klang Valley, Kuala Lumpur using positive matrix factorization, Atmos. Poll. Res., 2, 197–206, https://doi.org/10.5094/apr.2011.025, 2011.

Rai, P., Chakraborty, A., Mandariya, A. K., and Gupta, T.: Composition and source apportionment of PM_1 at urban site Kanpur in India using PMF coupled with CBPF, Atmos. Res., 178–179, 506–520, https://doi.org/10.1016/j.atmosres.2016.04.015, 2016.

Reff, A., Eberly, S. I., and Bhave, P. V.: Receptor modeling of ambient particulate matter data using positive matrix factorization: Review of existing methods, J. Air Waste Manage. Assoc., 57, 146–154, https://doi.org/10.1080/10473289.2007.10465319, 2007.

Richard, A., Gianini, M. F. D., Mohr, C., Furger, M., Bukowiecki, N., Minguillón, M. C., Lienemann, P., Flechsig, U., Appel, K., DeCarlo, P. F., Heringa, M. F., Chirico, R., Baltensperger, U., and Prévôt, A. S. H.: Source apportionment of size and time resolved trace elements and organic aerosols from an urban courtyard site in Switzerland, Atmos. Chem. Phys., 11, 8945–8963, https://doi.org/10.5194/acp-11-8945-2011, 2011.

Rudnick, R. L. and Gao, S.: Composition of the continental crust, Vol. 3, edited by: Rudnick, E., Book Section 2, 1–56, Elsevier Science, Philadelphia, 2003.

Taylor, S. R. and McLennan, S. M.: The geochemical evolution of the continental crust, Rev. Geophys., 33, 241–265, 1995.

Thorpe, A. and Harrison, R. M.: Sources and properties of non-exhaust particulate matter from road traffic: A review, Sci. Total Environ., 400, 270–282, https://doi.org/10.1016/j.scitotenv.2008.06.007, 2008.

Tian, S. L., Pan, Y. P., and Wang, Y. S.: Size-resolved source apportionment of particulate matter in urban Beijing during haze and non-haze episodes, Atmos. Chem. Phys., 16, 1–19, https://doi.org/10.5194/acp-16-1-2016, 2016.

Tremper, A. H., Font, A., Priestman, M., Hamad, S. H., Chung, T.-C., Pribadi, A., Brown, R. J. C., Goddard, S. L., Grassineau, N., Petterson, K., Kelly, F. J., and Green, D. C.: Field and laboratory evaluation of a high time resolution X-ray fluorescence instrument for determining the elemental composition of ambient aerosols, Atmos. Meas. Tech., 11, 3541–3557, https://doi.org/10.5194/amt-11-3541-2018, 2018.

Twigg, M. M., Di Marco, C. F., Leeson, S., van Dijk, N., Jones, M. R., Leith, I. D., Morrison, E., Coyle, M., Proost, R., Peeters, A. N. M., Lemon, E., Frelink, T., Braban, C. F., Nemitz, E., and Cape, J. N.: Water soluble aerosols and gases at a UK background site – Part 1: Controls of $PM_{2.5}$ and PM_{10} aerosol composition, Atmos. Chem. Phys., 15, 8131–8145, https://doi.org/10.5194/acp-15-8131-2015, 2015.

Ulbrich, I. M., Canagaratna, M. R., Zhang, Q., Worsnop, D. R., and Jimenez, J. L.: Interpretation of organic components from positive matrix factorization of aerosol mass spectrometric data, Atmos. Chem. Phys., 9, 2891–2918, https://doi.org/10.5194/acp-9-2891-2009, 2009.

Vallius, M.: Characteristics and sources of fine particulate matter in urban air. Ph.D. dissertation. Publications of the National Public Health Institute, Department of Environmental Health Kuopio, Finland, 2005.

Vecchi, R., Bernardoni, V., Cricchio, D., D'Alessandro, A., Fermo, P., Lucarelli, F., Nava, S., Piazzalunga, A., and Valli, G.: The impact of fireworks on airborne particles, Atmos. Environ., 42, 1121–1132, https://doi.org/10.1016/j.atmosenv.2007.10.047, 2008.

Visser, S., Slowik, J. G., Furger, M., Zotter, P., Bukowiecki, N., Canonaco, F., Flechsig, U., Appel, K., Green, D. C., Tremper, A. H., Young, D. E., Williams, P. I., Allan, J. D., Coe, H., Williams, L. R., Mohr, C., Xu, L., Ng, N. L., Nemitz, E., Barlow, J. F., Halios, C. H., Fleming, Z. L., Baltensperger, U., and Prévôt, A. S. H.: Advanced source apportionment of size-resolved trace elements at multiple sites in London during winter, Atmos. Chem. Phys., 15, 11291–11309, https://doi.org/10.5194/acp-15-11291-2015, 2015.

Vossler, T., Černikovský, L., Novák, J., and Williams, R.: Source apportionment with uncertainty estimates of fine particulate matter in Ostrava, Czech Republic using positive matrix factorization, Atmos. Pollut. Res., 7, 503–512, https://doi.org/10.1016/j.apr.2015.12.004, 2016.

Wahlström, J., Olander, L., and Olofsson, U.: Size, shape, and elemental composition of airborne wear particles from disc brake materials, Tribol. Lett., 38, 15–24, 2010.

Wang, Q., Qiao, L., Zhou, M., Zhu, S., Griffith, S., Li, L., and Yu, J. Z: Source apportionment of $PM_{2.5}$ using hourly measurements of elemental tracers and major constituents in an urban environment: investigation of time-resolution influence, J. Geophys. Res. : Atmos., 123, 5284–5300, https://doi.org/10.1029/2017JD027877, 2018.

Wang, Y., Zhuang, G., Xu, C., and An, Z.: The air pollution caused by the burning of fireworks during the lantern festival in Beijing, Atmos. Environ., 41, 417–431, https://doi.org/10.1016/j.atmosenv.2006.07.043, 2007.

Yu, L., Wang, G., Zhang, R., Zhang, L., Song, Y., Wu, B., Li, X., An, K., and Chu, J.: Characterization and source apportionment of $PM_{2.5}$ in an urban environment in Beijing, Aerosol Air Qual. Res., 13, 574–583, https://doi.org/10.4209/aaqr.2012.07.0192, 2013.

Zhang, R., Jing, J., Tao, J., Hsu, S.-C., Wang, G., Cao, J., Lee, C. S. L., Zhu, L., Chen, Z., Zhao, Y., and Shen, Z.: Chemical characterization and source apportionment of $PM_{2.5}$ in Beijing: seasonal perspective, Atmos. Chem. Phys., 13, 7053–7074, https://doi.org/10.5194/acp-13-7053-2013, 2013.

Zhao, W. and Hopke, P. K.: Source apportionment for ambient particles in the San Gorgonio wilderness, Atmos. Environ., 38, 5901–5910, https://doi.org/10.1016/j.atmosenv.2004.07.011, 2004.

Zhou, S., Davy, P. K., Huang, M., Duan, J., Wang, X., Fan, Q., Chang, M., Liu, Y., Chen, W., Xie, S., Ancelet, T., and Trompetter, W. J.: High-resolution sampling and analysis of ambient particulate matter in the Pearl River Delta region of southern China: source apportionment and health risk implications, Atmos. Chem. Phys., 18, 2049–2064, https://doi.org/10.5194/acp-18-2049-2018, 2018.

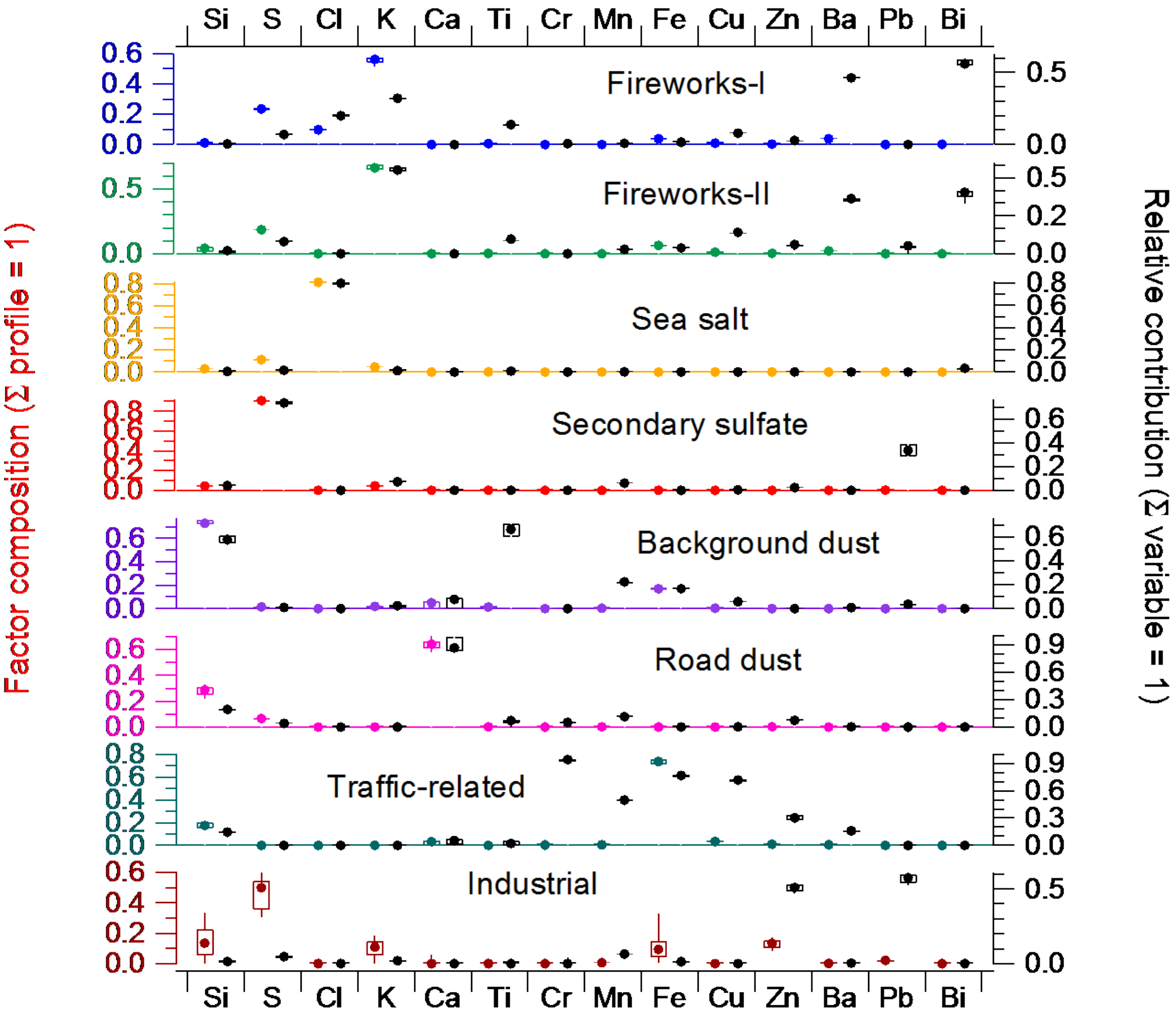

Figure 1: Source profiles of PMF results. The data and their corresponding uncertainty are given as box-whisker plot (bottom to top: p10-p25-p50-p75-p90) of good solutions from bootstrap runs. The left y-axis represents the normalized variable intensity in row-wise (presented in coloured box whisker plot) for each factor in ng ng^{-1}, the right y-axis represents the fraction of the total predicted concentration for a given variable (indicated in black box-whisker plot). 5

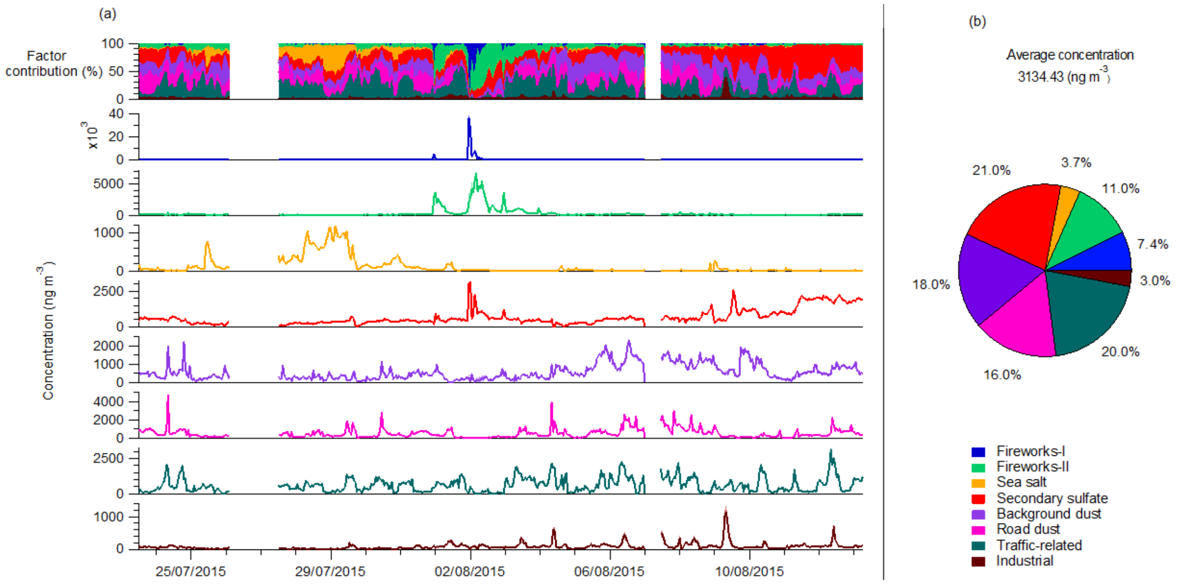

Figure 2: (a) Time series of the PM_{10} elemental sources and relative contributions of the different sources over time; shaded areas indicate the uncertainties (interquartile) of selected bootstrap runs; (b) Mean relative contributions of PM_{10} elemental sources.

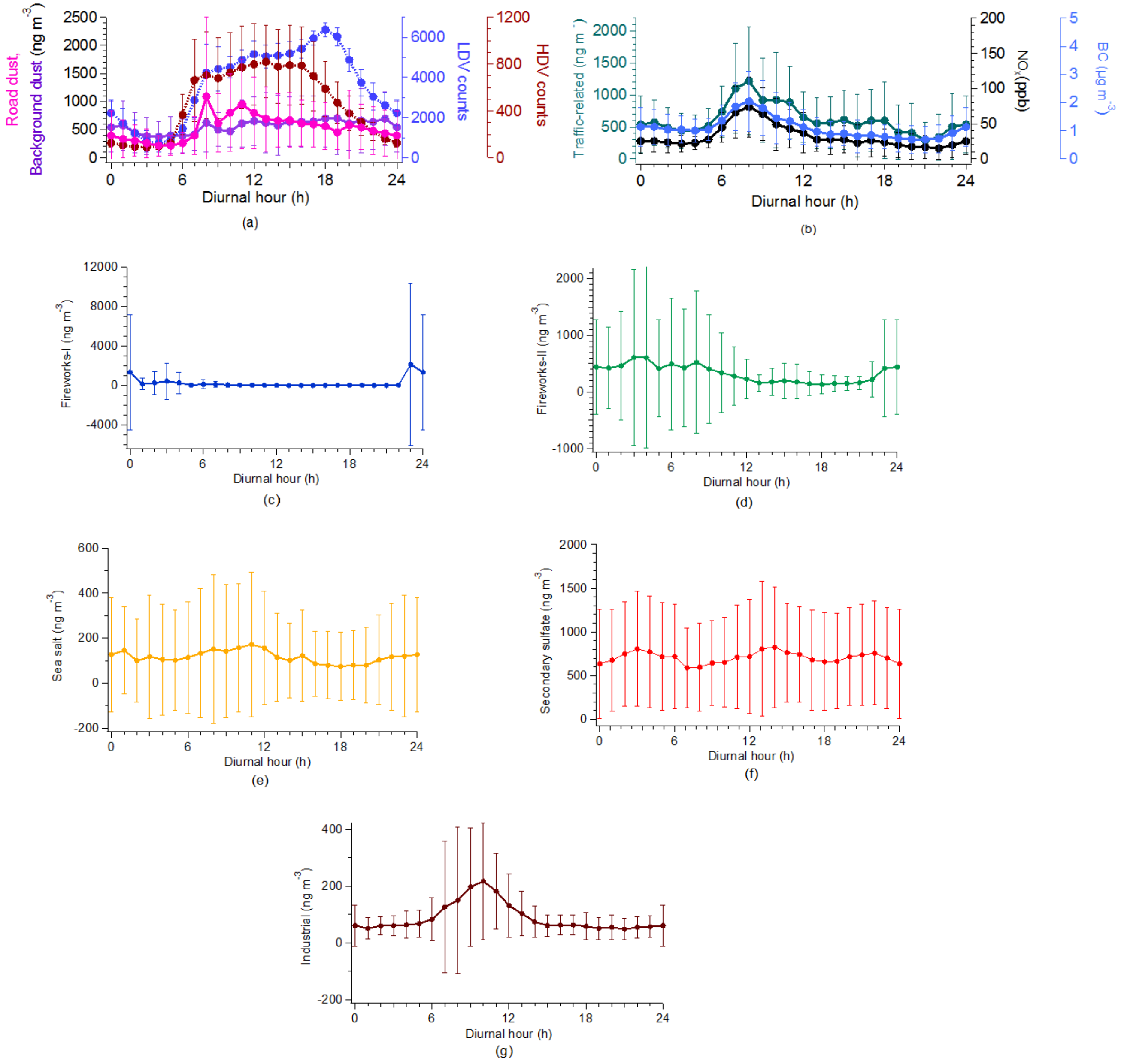

Figure 3: Mean diurnal patterns of the factors and of some corresponding external tracers with error bars (one standard deviation).

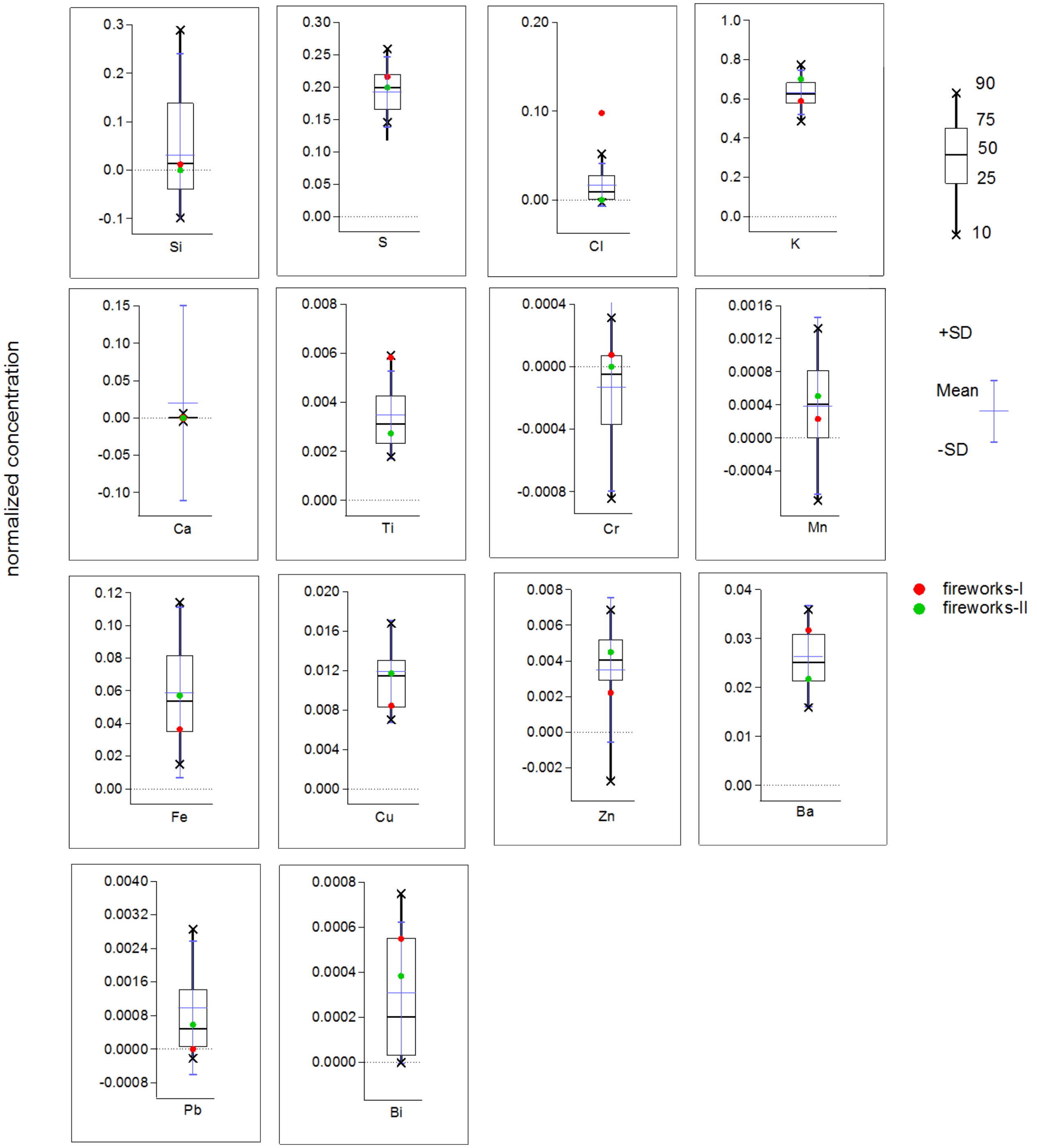

Figure 4: Representation of fireworks data points (normalized concentration) in terms of mean, median, 10-25-75-90th percentiles (bottom to top) and one standard deviation. Red and green dots denote the factor composition of fireworks-I and fireworks-II, respectively.